ORIGINAL PAPER

Critical Field Analysis and Magnetocaloric Effect of A-Site Double-Doped Manganese Oxide La$_{0.9}$EuSr$_{0.1}$MnO$_3$

Hongwei Chen[1] · Cheng Li[1] · Jianjun Zhao[1] · Yi Lu[1] · Fengze Cao[1] · Wenxing Wang[1] · Lin Zheng[1] · Xiang Jin[1]

Abstract

Polycrystalline La$_{0.9-x}$Eu$_x$Sr$_{0.1}$MnO$_3$ ($x=0.000$, 0.025) samples were prepared using a traditional high temperature solid-state reaction method. The effects of double doping of cationic Eu^{3+} and Sr^{2+} on the preformed clusters, critical field behavior, and change of magnetic entropy of LaMnO$_3$ were studied systematically. The results show that polycrystalline La$_{0.9-x}$Eu$_x$Sr$_{0.1}$MnO$_3$ ($x=0.000$, 0.025) samples are orthogonal crystal structures with a good unidirectionality and the space group of the polycrystalline samples is *Pbnm*. As the temperature increased from 15 to 380 K, the polycrystalline La$_{0.9-x}$Eu$_x$Sr$_{0.1}$MnO$_3$ ($x=0.000$, 0.025) sequentially displayed the characteristics of cluster spin glass, ferromagnetic phase, preformed cluster, and paramagnetic phase. For both La$_{0.9-x}$Eu$_x$Sr$_{0.1}$MnO$_3$ samples, the second-order phase transition occurs near Curie temperature. The critical index of the undoped parent compound and doped sample fitted best to the mean-field model and 3D-Heisenberg model, respectively. At an applied magnetic field of 7 T, the maximum absolute values of the magnetic entropy changes of the two samples were 2.76 ± 0.002 J·kg^{-1}·K^{-1} and 2.81 ± 0.002 J·kg^{-1}·K^{-1}, respectively, and the temperature corresponding to the maximum absolute values of the magnetic entropy change was approximately 130 K. The magnetic refrigerant capacities (RC) of the two La$_{0.9-x}$Eu$_x$Sr$_{0.1}$MnO$_3$ samples were 436.01 ± 0.002 J·kg^{-1} and 438.09 ± 0.002 J·kg^{-1}, respectively. Our results revealed that the changes in magnetic entropy and magnetic refrigerating capacity of the doped sample increased compared to the parent sample, suggesting that the double-doped manganese oxide La$_{0.9-x}$Eu$_x$Sr$_{0.1}$MnO$_3$ samples can be used as magnetic refrigerants in the medium temperature range of 80 to 250 K.

Keywords Perovskite manganese oxide · Doping · Preformed cluster · Critical behavior · Magnetic entropy change · Refrigeration capacity

Abbreviations

RC	Refrigerant capacities
MCE	Magnetocaloric effects
DE	Double exchange
XRD	X-ray diffraction
VSM	Vibrating sample magnetometer
ZFC	Zero field cooling
K-F	Kouvel-Fisher method

1 Introduction

Magneto-refrigeration technology based on magnetocaloric effects (MCE) is important for energy saving, is environmentally friendly, and can replace traditionally used refrigeration technologies [1–3]. Previous studies show that the rare earth element Gd has a large MCE. However, the use of Gd as a magnetic refrigerant is limited due to its high price [4–6]. Doped manganese oxides have attracted some attention in the field of magnetic refrigeration research. Studies reveal that the double-doped manganese oxide with the formula R$_{1-x}$A$_x$MnO$_3$, where R is a trivalent rare-earth cation, and A is a divalent alkaline earth cation, has a large MCE.

Furthermore, double-doped manganese oxides showed advantages compared to Gd and other magnetic refrigerating materials. The double-doped manganese oxides are low-cost and convenient to prepare, while they exhibit high chemical stability, high resistance, and favorable eddy current reduction [3, 5].

The transport and magnetic properties of manganese oxide can be explained by Zener double exchange (DE) [3, 7–9]. It is well known that the DE is very sensitive to the Mn–O bond length and the Mn–O–Mn bond angle and is a function of the average radius of the ions at A or Mn sites. If the ion at the A site is substituted with a rare earth element with a different ionic

✉ Xiang Jin
  jin122120@163.com

1 Inner Mongolia University of Science and Technology, Baotou 014030, Inner Mongolia, China

radius, internal stress changes in the crystal lattice lead to the deformation of the MnO_6 octahedron. This results in a decrease in the Mn–O–Mn bond angle [1–3, 9]. A difference of the Neel temperature was achieved with varying degrees of the average radius of the cations, which is important for equivalent ion valence substitutions [1, 8–10] except for the change of the Mn^{3+}/Mn^{4+} ratio. Thus, changing the average anion radius $<r_A>$ via doping is beneficial for the adjustment of the ferromagnetic–paramagnetic transition temperature and the regulation of MCE [8, 11]. The ferromagnetic–paramagnetic phase transition temperature of the Sr-doped manganese oxides was higher [1, 8].

Numerous efforts were made to dope the A site. In our previous study, the magnetic and magnetocaloric properties of $La_{0.9-x}Eu_xSr_{0.1}MnO_3$ ($x=0.05$) were investigated. Compared to the undoped $La_{0.9}Sr_{0.1}MnO_3$ sample, the magnetic entropy change in a 7-T magnetic field and the RCP decreased to 2.53 J· K^{-1}· kg^{-1} and 354.93 J· kg^{-1}. The doping levels were further decreased to $x=0.025$ in order to improve the properties of doped La0.9-xEuxSr0.1MnO3, In this study, the MCE and critical field behavior of the $La_{0.9-x}Eu_xSr_{0.1}MnO_3$ ($x=0.000$, 0.025) samples were investigated after adjusting the average radius of the cation at the site A.

2 Material and Methods

The polycrystalline $La_{0.9-x}Eu_xSr_{0.1}MnO_3$ ($x=0.000$, 0.025) samples were prepared using a traditional high-temperature solid-phase reaction. High purity (≥ 99.9 wt%) La_2O_3, Eu_2O_3, $SrCO_3$, and $MnCO_3$ were strictly weighed following the stoichiometry ratio and then ground with an agate mortar. The mixture was sintered twice for 12 h at atmospheric pressure and a temperature of 1000 °C and 1100 °C, respectively, and was ground between two sintering steps. The sample was ground for a final round at the end and pressed into a circular pellet with a diameter of 10 mm and a thickness of ~2 mm using a pellet press set. The pellets were sintered at 1250 °C for 24 h at atmospheric pressure in a tube sintering furnace, and bright, high-quality samples with smooth and crack-free surfaces were obtained. An X-ray diffractometer (XRD) was used to examine the crystalline structure and quality of the samples. The magnetic properties of the samples were obtained using the multifunction physical property measurement system (US Quantum Design, PPMS) with a vibrating sample magnetometer (VSM) module.

3 Results and Discussion

The sample quality and crystal structure of the polycrystalline $La_{0.9-x}Eu_xSr_{0.1}MnO_3$ ($x=0.000$, 0.025) samples were measured using an X-ray diffractometer at room temperature. As shown in Fig. 1, the XRD patterns revealed that
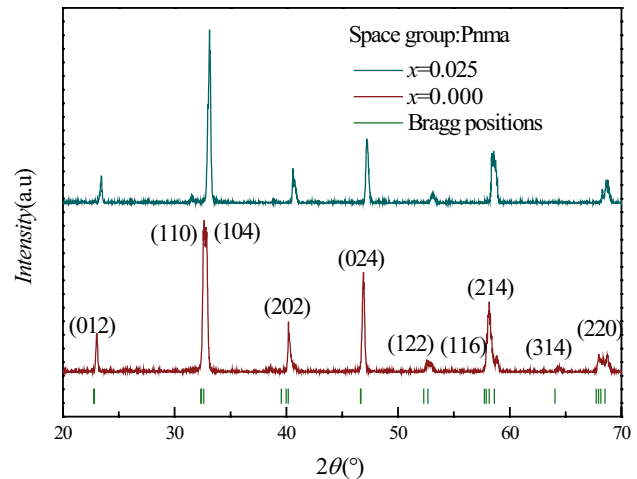
Fig. 1 XRD patterns of polycrystalline $La_{0.9-x}Eu_xSr_{0.1}MnO_3$ samples with $x=0.000$ and 0.025 at room temperature

all samples are in the space group of *Pbnm* and have an orthogonal crystal structure with good unidirectionality. The Eu^{3+} doping did not affect the spatial structure compared to its parent compound. The XRD results showed the presence of extremely small amounts of Eu_2O_3 in the LSMO matrix. However, Eu_2O_3 impurities did not affect the changes of the adiabatic temperature (ΔT_{ad}) since the lattice-specific heat dominates. Table 1 shows the lattice parameters and c/a of the $La_{0.9-x}Eu_xSr_{0.1}MnO_3$ samples with $x=0.000$ and 0.025. The results show that the doping decreased the lattice parameters a and c and increased b. The slight change in the lattice parameters with doping was attributed to the radius difference between La^{2+} and Eu^{3+} [2, 12–14] since the La^{2+} radius (0.117 nm) was larger than the Eu^{3+} radius (0.0947 nm), which resulted in a shrinkage of the unit cell volume after Eu^{3+} doping.

The distortion of the crystalline structure was measured using the tolerance factor t [15], which was calculated as

$$t = (r_A + r_O)/2^{1/2}(r_{Mn} + r_O) \tag{1}$$

where r_A, r_O, r_{Mn} are the radii of the rare earth ion, oxygen ion, and manganese ion, respectively. The calculated results show that the tolerance factors of the polycrystalline $La_{0.9-x}Eu_xSr_{0.1}MnO_3$ samples with $x=0.000$ and 0.025 were $t_{0.000}=0.876$ and $t_{0.025}=0.875$, respectively. Distortion occurs when $t=0.75\sim0.9$, at which the symmetry decreases, but the orthogonal crystal structure is stable [16]. After the Eu^{3+} doping, the tolerance factor decreased slightly, and the degree of the structure distortion of the sample increased.

The magnetization was a function of temperature (*M-T* curve) of the $La_{0.9-x}Eu_xSr_{0.1}MnO_3$ samples ($x=0.000$, 0.025) at a magnetic field of 0.05 T, as shown in Fig. 2. The zero field cooling (ZFC) and zone cooling (FC) curves of each sample were shown in Fig. 2. The inset presents the d*M*/d*T*

Table 1 Crystal parameters and c/a of the $La_{0.9-x}Eu_xSr_{0.1}MnO_3$ samples with $x=0.000$ and 0.025

x	a/nm	b/nm	c/nm	V/nm^3	c/a
0.000	0.553 ± 0.0002	0.548 ± 0.0002	0.779 ± 0.0003	0.236 ± 0.0001	1.410 ± 0.0001
0.025	0.549 ± 0.0002	0.552 ± 0.0002	0.777 ± 0.0002	0.235 ± 0.0003	1.416 ± 0.0002

versus T curve. The results reveal that at high temperatures, these two $La_{0.9-x}Eu_xSr_{0.1}MnO_3$ samples were paramagnetic. The magnetic property of the samples changed from paramagnetic to ferromagnetic with increasing temperatures. At Curie temperatures, $Tc1 \approx 130$ K and $Tc2 \approx 120$ K, the magnetization increased dramatically, and the samples had ferromagnetic properties [17–21]. After Eu^{3+} doping, the decrease of the average ionic radius increased the lattice distortion, decreased the Mn–O-Mn bond angle, and reduced the ferromagnetic interaction between Mn^{3+} and Mn^{4+} through oxygen, resulting in a decrease of the Curie temperature and magnetization [1, 22, 23]. As the temperature in the lower temperature region further decreased, the ZFC and FC curves of the samples deviated from each other. This could be attributed to the competition between the ferromagnetic and antiferromagnetic states of the molecules. The deviations of the ZFC and FC curves of the samples from each other indicate a cluster spin-glass behavior [2].

At a magnetic field of 0.05 T, the magnetic susceptibility times temperature (χT) *versus T* curves of the two polycrystalline $La_{0.9-x}Eu_xSr_{0.1}MnO_3$ samples (with $x=0.000$ and 0.025) are shown in Fig. 3. The χT decreased as the temperature increased and reached the maximum near 105 K before it rapidly decreased. Thus, the Neel temperature obtained is $T_{N1} \approx 105$ K. The samples are antiferromagnetic below the Neel temperature, which is consistent

with our previous results. The Neel temperature for the Eu^{3+}-doped samples was slightly lower than the undoped sample.

The inverse of the magnetic susceptibility (χ^{-1}) *versus T* and the Curie–Weiss fitting curves of $La_{0.9-x}Eu_xSr_{0.1}MnO_3$ ($x=0.000$, 0.025) samples was calculated at a magnetic field of 0.05 T (Fig. 4). The Curie–Weiss law for fitting was calculated as follows [24–27].

$$\chi(T) = C/(T - \theta)$$

where C is the Curie constant and θ is the Curie–Weiss temperature. The fitting results revealed that the Curie's temperature of the two $La_{0.9-x}Eu_xSr_{0.1}MnO_3$ samples (with $x=0.000$ and 0.025) were $\theta 1 \approx 200$ K and $\theta 2 \approx 190$ K, respectively. In the temperature regions of 130–285 K and 120–290 K, the χ^{-1}-T curves of both samples deviated from the Curie–Weiss law as depicted in Fig. 4. This is ascribed to the antiferromagnetic competition within the system, resulting in the anti-parallel arrangement of the ferromagnetic clusters. This suggests that there are preformed clusters in the polycrystalline samples [2]. Combined with our other results from Fig. 2, we discovered that an increase in temperature within the temperature regions of 15–105 K and 15–96 K resulted in antiferromagnetic phase characteristics of both samples. Within the temperature regions of 105–130 K and 96–120 K, the samples were ferromagnetic. At 130–285 K and 120–290 K, the samples presented as preformed clusters. The $La_{0.9-x}Eu_xSr_{0.1}MnO_3$ samples (with $x=0.000$ and 0.025) presented as pure paramagnetic materials above the temperature of 285 K and 290 K, respectively.

The experimental effective paramagnetic moment was obtained by [3, 16]

$$\mu_{eff}^{exp} = (3k_BC/N_{Av})^{1/2} \tag{2}$$

where the Avogadro constant $N_{Av}=6.023 \times 10^{23}$ mol^{-1} and the Boltzmann constant $k_B=1.38016 \times 10^{-23}$ J· K^{-1}.
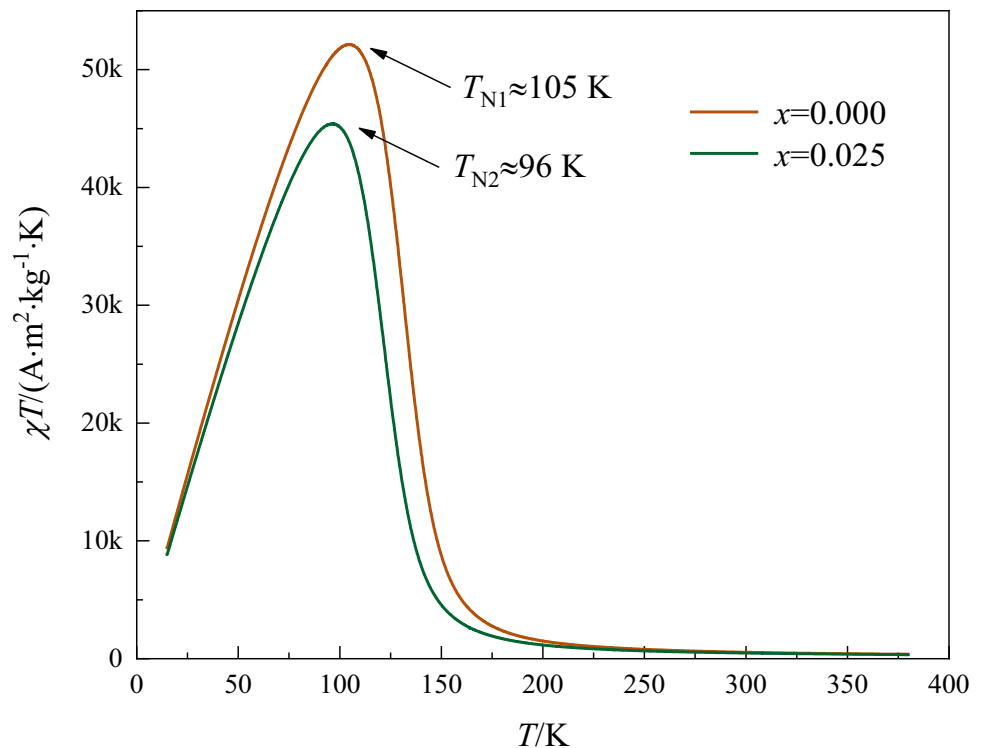
The theoretical effective magnetic moment was determined by [2, 4, 28]

$$\mu_{eff}^{the} = \left[0.1\mu_{eff}^2(Mn^{4+}) + x\mu_{eff}^2(Eu^{3+}) + (0.9-x)\mu_{eff}^2(Mn^{3+})\right]^{1/2} \tag{3}$$

Table 2 shows the Curie constant C, Curie temperature θ, experimental effective paramagnetic moment, and the theoretical effective magnetic moment of the $La_{0.9-x}Eu_xSr_{0.1}MnO_3$ samples with $x=0.000$ and 0.025 at a
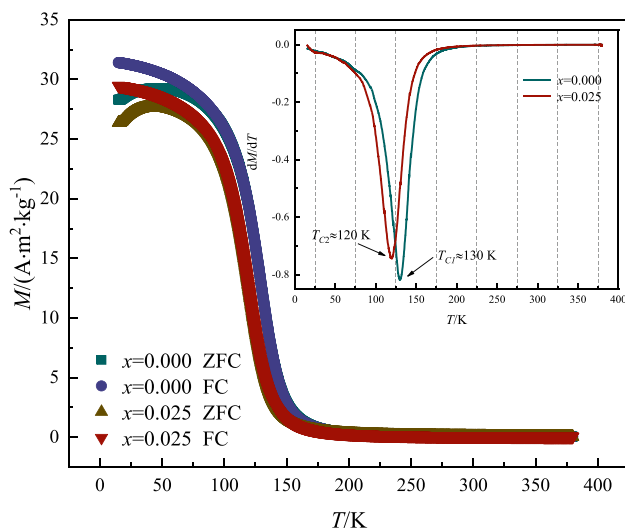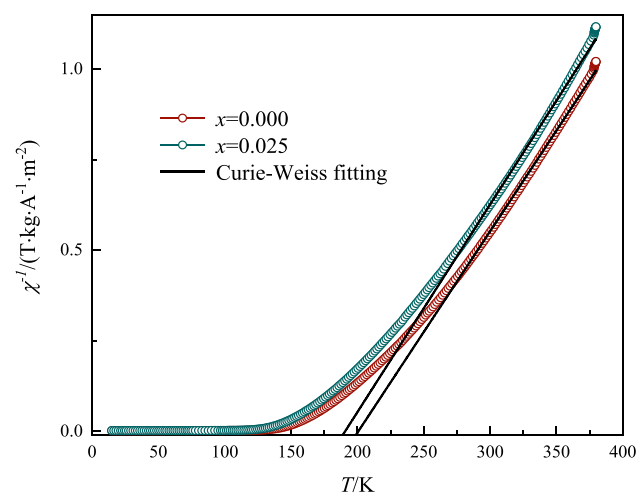

Fig. 2 Magnetization *versus* temperature (*M-T*) curve of $La_{0.9-x}Eu_xSr_{0.1}MnO_3$ ($x=0.000$, 0.025) samples at a magnetic field of 0.05 T. The inset is d*M*/d*T versus T* curve

Fig. 3 Magnetic susceptibility times temperature (χT) *versus* T curves of the polycrystalline La$_{0.9-x}$Eu$_x$Sr$_{0.1}$MnO$_3$ samples with $x = 0.000$ and 0.025 at a magnetic field of 0.05 T

magnetic field of 0.05 T. The difference between the experimental and theoretical effective paramagnetic moments resulted from the existence of ferromagnetopolaron in the paramagnetic materials.

A series of isothermal magnetization measurements were carried out near the Curie temperature to investigate the magnetocaloric effect of the La$_{0.9-x}$Eu$_x$Sr$_{0.1}$MnO$_3$ ($x = 0.000$, 0.025) samples. Figure 5a, b illustrate the isothermal magnetization curves (*M-H* curves) of the two samples.

Fig. 4 Inverse of magnetic susceptibility (χ^{-1}) *versus* T curves of La$_{0.9-x}$Eu$_x$Sr$_{0.1}$MnO$_3$ samples with $x = 0.000$ and 0.025 at a magnetic field of 0.05 T

At the same temperature, the magnetization of the samples increased as the external magnetic field increased. Under the same magnetic field, the system was subjected to more intense thermal perturbation with increasing temperatures, leading to the magnetization of the samples decrease [2, 29–31]. Furthermore, the *M-H* curve of the sample tended to be linear at high temperatures, indicating that the paramagnetic state of the sample was most prevalent in the high-temperature region. In contrast, the magnetization of the two samples rapidly increased and tended to be saturated at low temperatures, indicating a predominantly ferromagnetic phase.

Figure 5c, d illustrate the isothermal Arrott curves (*H/M-M²* curves) of the La$_{0.9-x}$Eu$_x$Sr$_{0.1}$MnO$_3$ samples with $x = 0.000$ and 0.025. No obvious S shape and negative slope were observed for the curves. Following the Banerjee criterion [32–35], the paramagnetic-ferromagnetic transition of the two samples near T_c was a second-order phase transition.

To study the second-order phase transition of the La$_{0.9-x}$Eu$_x$Sr$_{0.1}$MnO$_3$ samples with $x = 0.000$ and 0.025, the mean field, three-dimensional Heisenberg, three-dimensional Ising, and tri-critical models were used to fit the magnetization curves of the samples. Figure 6a show the fitting results of the magnetization of the La$_{0.9-x}$Eu$_x$Sr$_{0.1}$MnO$_3$ sample with $x = 0.000$ using the mean field, three-dimensional Heisenberg, three-dimensional Ising, and tri-critical models, respectively, at temperatures ranging from 120 to 140 K with an incremental increase of 2 K. The fitting results revealed that for the

Table 2 Curie temperature T_C, Curie–Weiss constant C, paramagnetic Curie temperature θ, and the experimental and theoretical magnetic, paramagnetic moments of the $La_{0.9-x}Eu_xSr_{0.1}MnO_3$ samples with $x = 0.000$ and 0.025 at a magnetic field of 0.05 T

| Sample	T_C /K	$C/(10^{24}\ \mu_B\ K\cdot mol^{-1})$	θ/K	μ_{eff}^{exp}/μ_B	μ_{eff}^{the}/μ_B
$La_{0.9}Sr_{0.1}MnO_3$	130	4.59 ± 0.002	200	5.83 ± 0.002	4.81 ± 0.001
$La_{0.875}Eu_{0.025}Sr_{0.1}MnO_3$	120	4.46 ± 0.002	190	5.75 ± 0.002	4.77 ± 0.003

sample with a doping amount of 0.000 ($x = 0.000$), the fitting curves of the mean field and three-dimensional Heisenberg and Ising models were parallel to the experimental curve spanning a large range of temperatures and $H \cdot M^{-1}$. The tri-critical model fittings showed a divergence from the experimental magnetization curve. The mean field model had the best fitting for the experimental magnetization curve of the sample. Figure 6b show the fitting results of the magnetization of the second $La_{0.9-x}Eu_xSr_{0.1}MnO_3$ sample with $x = 0.025$ using again the mean field, three-dimensional Heisenberg, and Ising,

and tri-critical models, respectively, at temperatures ranging between 112 and 152 K with an incremental increase of 4 K. The results from Fig. 6b illustrated that for the $La_{0.9-x}Eu_xSr_{0.1}MnO_3$ sample with $x = 0.025$, the experimental magnetization curve fits the three-dimensional Ising model the best compared to other models.

To further examine which model fits the $La_{0.9-x}Eu_xSr_{0.1}MnO_3$ ($x = 0.000$, 0.025) samples best, the critical exponents β, γ, and δ [1, 36] of the samples were obtained using the Kouvel-Fisher (K-F) method. β is the critical exponent associated with the critical behavior of
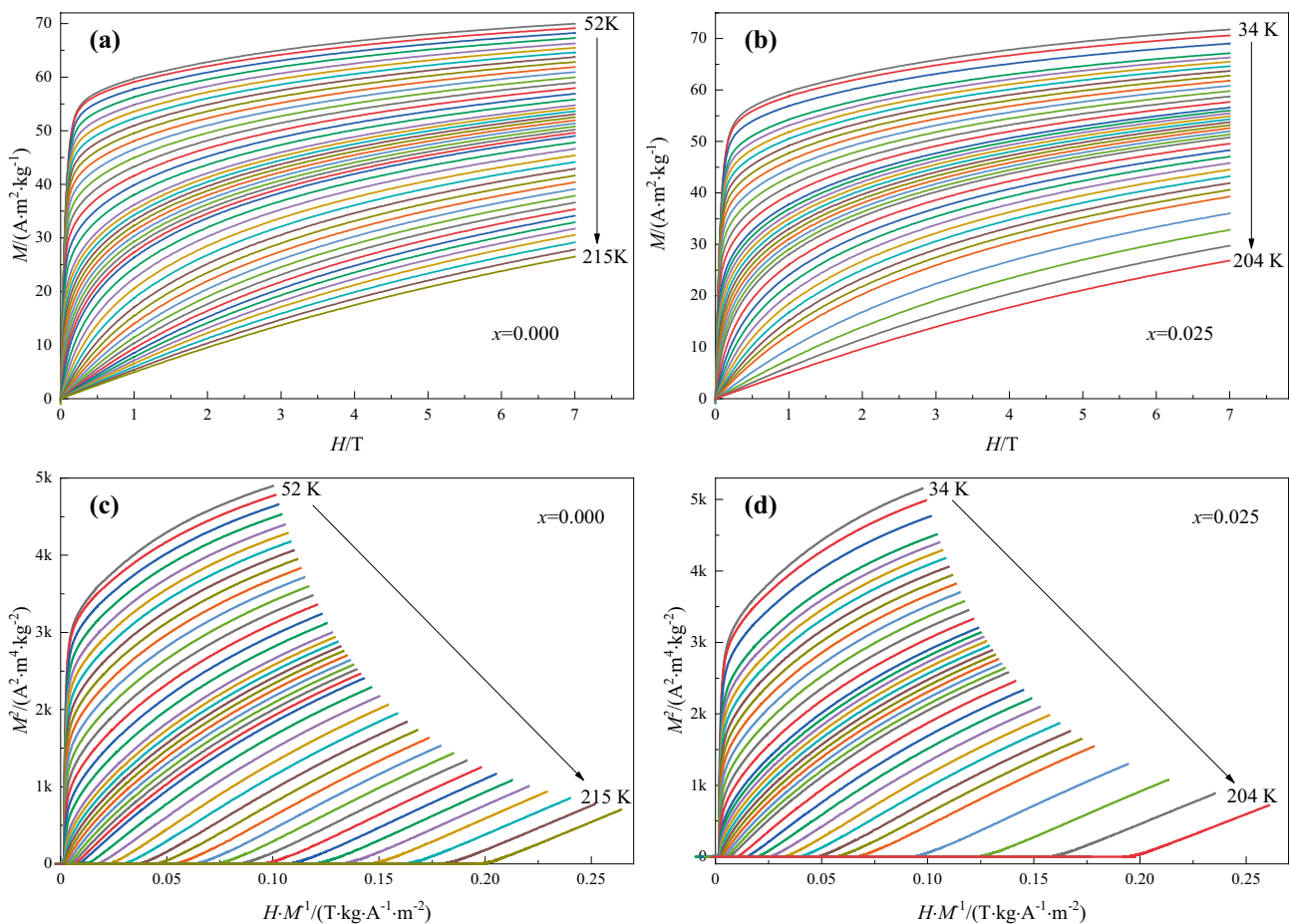
Fig. 5 **a** and **b** Magnetization curves (*M-H* curves) of the $La_{0.9-x}Eu_xSr_{0.1}MnO_3$ samples with $x = 0.000$ and 0.025, respectively, at varied temperatures. **c** and **d** Isothermal Arrott curves of the $La_{0.9-x}Eu_xSr_{0.1}MnO_3$ samples with $x = 0.000$ and 0.025, respectively, at varied temperatures
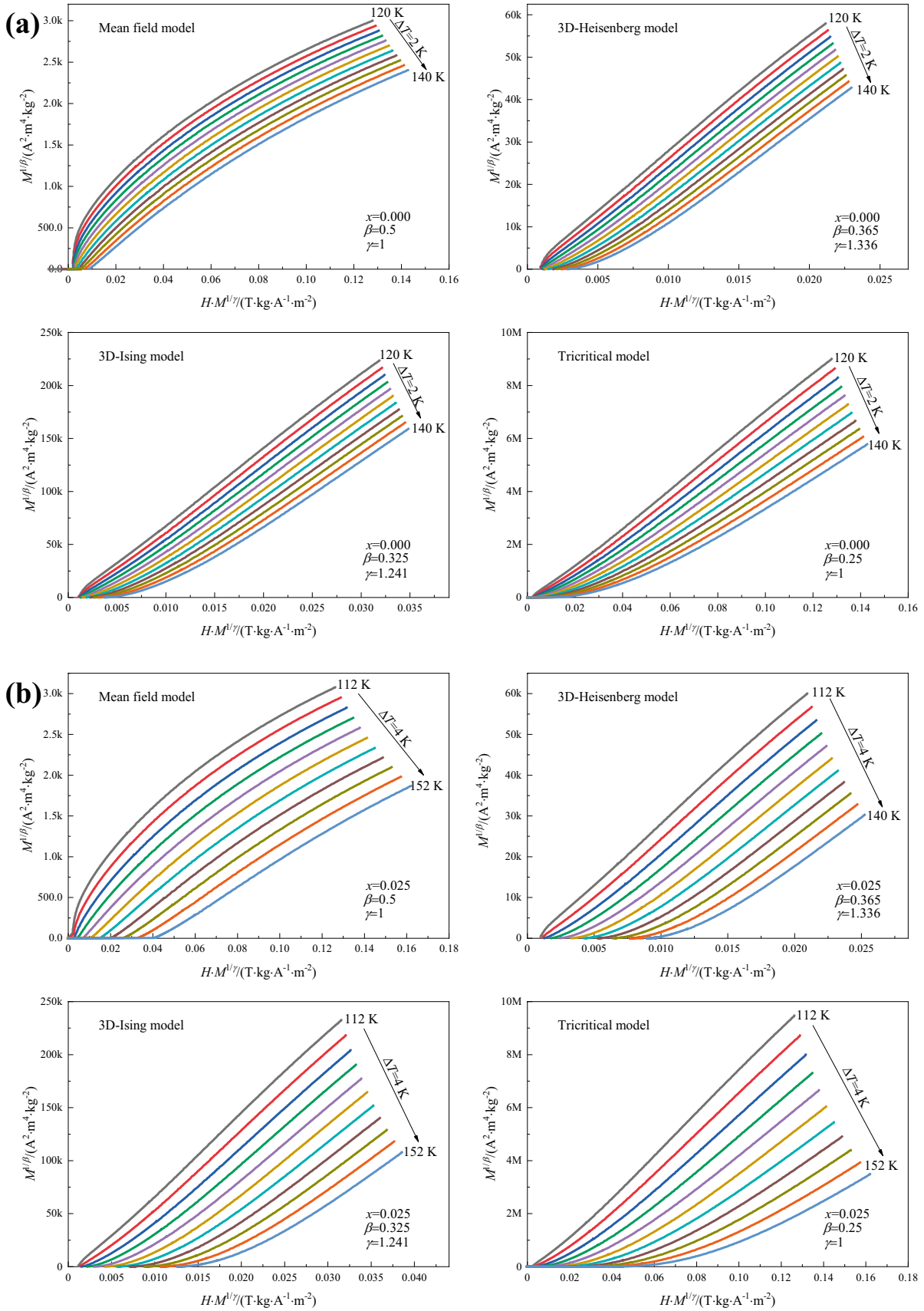
◀ **Fig. 6 a** The fitting results of the magnetization of the La$_{0.9-x}$Eu$_x$Sr$_{0.1}$MnO$_3$ sample with $x=0.000$ using the mean field, three-dimensional Heisenberg, three-dimensional Ising, and tri-critical models, respectively, at temperatures from 120 to 140 K with an incremental increase of 2 K. **b** The fitting results of the magnetization of the La$_{0.9-x}$Eu$_x$Sr$_{0.1}$MnO$_3$ sample with $x=0.025$ using the mean field, three-dimensional Heisenberg, three-dimensional Ising, and tri-critical models, respectively, at temperatures from 112 to 152 K at an increment step of 4 K

spontaneous magnetization; γ is the critical exponent related to the critical behavior of the magnetic susceptibility with no applied magnetic field; δ is the critical exponent of the state function. The Kouvel-Fisher equations are as follows:

$$M_s(T)\left[dM_s(T)/dT\right]^{-1} = \left(T-T_c\right)/\beta \tag{4}$$

$$\chi_0^{-1}(T)\left[d\chi_0^{-1}(T)/dT\right]^{-1} = \left(T-T_c\right)/\gamma \tag{5}$$

$$\delta = 1 + (\gamma/\beta) \tag{6}$$

where M_S is the spontaneous magnetization, χ_0^{-1} is the susceptibility at a zero magnetic field. The Arrott plots in the temperature ranges of $T \leq Tc$ and $T > Tc$ were linearly fitted, and the intercepts obtained from the fitting curves are M_S^2 and χ_0^{-1}, respectively. Figure 7A(a), B(a) illustrates the spontaneous magnetization *versus* temperature (*Ms-T*) plots below the Curie temperature, and Figs. 7A(b), B(b) shows the $Ms(T)\cdot(dMs/dT)^{-1}$ *versus* T curves. Figures 7A(c) to (d), B(c) to (d) show the inverse of the magnetic susceptibility at a zero magnetic field versus temperature and $\chi_0^{-1}(d\chi_0^{-1}/dT)$ *versus* T plots with the temperature that is higher than the Curie temperature. The $1/\beta$ value represents the slope of the fitted $Ms(T)\cdot(dMs/dT)^{-1}$ *versus* T curve, as shown in Eq. (4). Based on the slope, we determined that the $\beta1$ of the polycrystalline La$_{0.9-x}$Eu$_x$Sr$_{0.1}$MnO$_3$ sample with the doping amount $x=0.000$ was 0.52 ± 0.02. The $1/\gamma$ was expressed as the slope of the $(d)\chi_0^{-1}(d\chi_0^{-1}/dT)$ *versus* T fitting curve, as shown in Eq. (5), and was $\gamma1 = 1.02\pm0.02$. Based on Eq. (6), we obtained $\delta1 = 2.96\pm0.01$. Comparing the results with the data from the models, the results of the sample fit best with the mean field model. Furthermore, the critical exponents for the Eu^{3+}-doped sample, $\beta2=0.368\pm0.02$, $\gamma2=1.303\pm0.02$, and $\delta2=4.54\pm0.01$, fit best with the 3D- Heisenberg model, which is consistent with the previous results.

The magnetic equation of state is a relationship between the variables M(H,ε), H, and T. From the scaling hypothesis, the equations is as follow:

$$M(H,\varepsilon) = \varepsilon^\beta f \pm \left(H/\varepsilon^{\beta+\gamma}\right) \tag{7}$$

where f stands for regular analytic function, f + for $T > T_C$, and f- for $T < T_C$. ε is the reduced temperature, $(T-T_C)/T_C$. The scaled $M/|\varepsilon|^\beta$ is plotted as a function of the scaled $H/|\varepsilon|^{\beta+\gamma}$. Two individual branches appeared in the vicinity of T_C, confirming that the critical parameters determined are in good conformity to the scaling hypothesis. The two different curves in ln $(M/|\varepsilon|^\beta)$ as a function of $\ln(H/|\varepsilon|^{\beta+\gamma})$ strongly support the accuracy of obtained values of the critical exponents and T_C as shown in the inset of Fig. 8.

Critical exponents affect how magnetic caloric reactions respond. According to Oesterreicher et al. [1], the equation for field dependence of change in magnetic entropy ΔS_M for the second-order magnetic phase transition is

$$\left|\Delta S_M^{\max}\right| = a(H)^n \tag{8}$$

where *a* is a constant and *n* depends upon the magnetic state of the compound. *n* can be calculated by the logarithmic derivative of the ΔS_M to the magnetic field:

$$n = \frac{d\ln\Delta S_M}{d\ln H} \tag{9}$$

n reaches about "2" in the paramagnetic region ($T > T_C$) and about "1" in ferromagnetic region (for $T < T_C$). *n* is field independent at T_C and can be found by

$$n = 1 + \frac{\beta-1}{\beta+\gamma} = 1 + \frac{1}{\delta}(1-\frac{1}{\beta}) \tag{10}$$

Figure 9 uses Eq. (9) to demonstrate how temperature affects the exponent n (T, H) at different fields. The figure shows that n changes with the field over the temperature range, and its values are very similar above the Tc. n approaching "2″ for temperatures greater than Tc is a consequence of the Curie–Weiss law, suggesting that the magnetization has a linear field dependence in the higher temperature range. At $T < T_C$, n is approximately ''1." The n at Curie temperature (T_C) can be calculated with critical exponents β and γ with Eq. (10). Mean field theory and 3D-Heisenberg theory explains that a minimum value of n at $T = T_C$ is projected to be around 0.67 and 0.637 [37]. In our compounds, n values near the temperature T_C were measured to be 0.68 ± 0.001 and 0.623 ± 0.002 for $x=0.000$ and 0.025, respectively. Our simulated values of n are very close to the theoretical values of n near Curie temperature, indicating that the critical model we built is reasonable. Before doping, the model is an average field model, and the interaction of the magnet falls into the magnetic field fluctuation effect. After doping, the model changed to the Heisenberg model, and the apparent critical fluctuation near Curie temperature (Tc) led to the critical indices $\beta < 0.5$
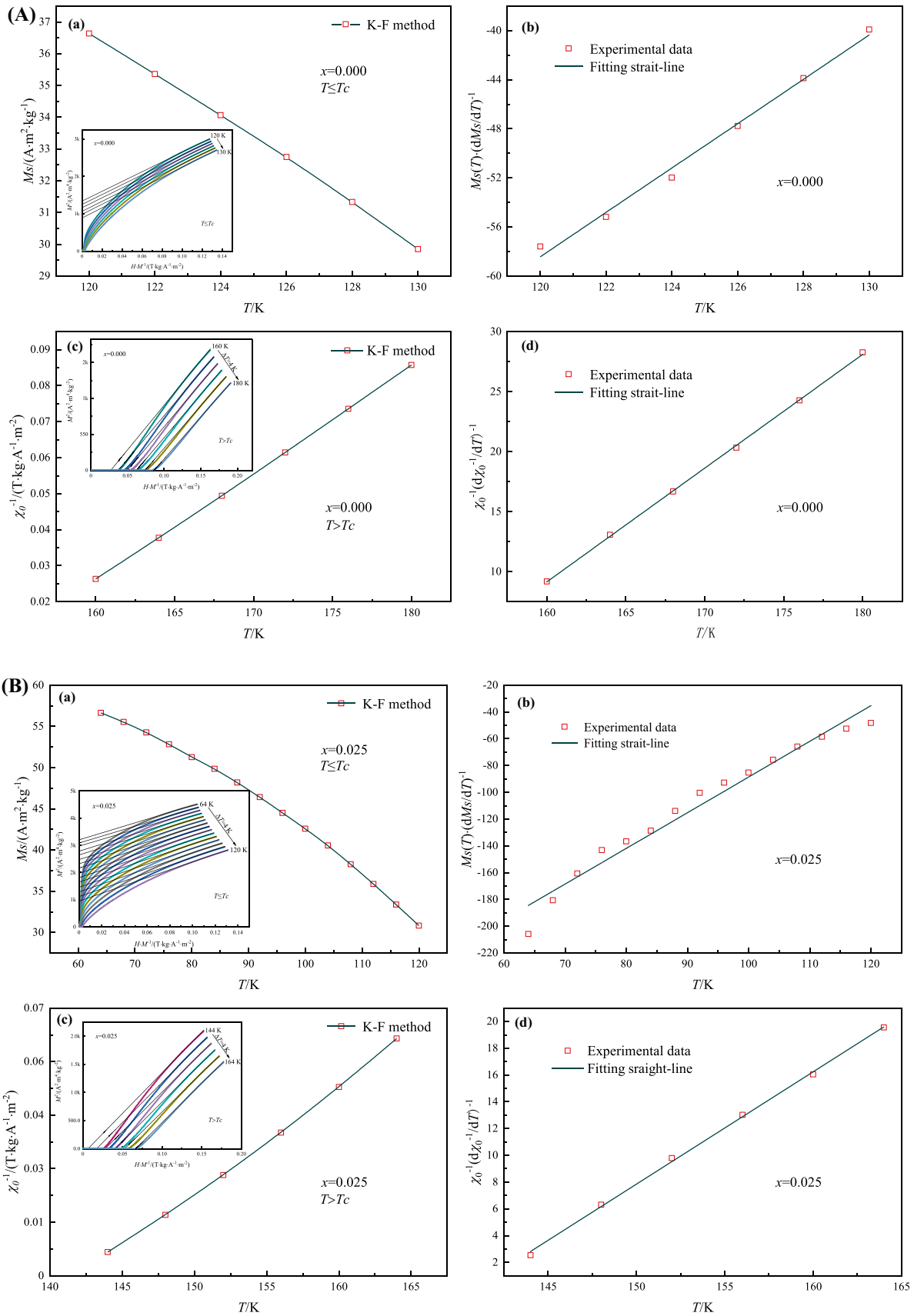
◄**Fig. 7** Spontaneous magnetization (*Ms*) of the La$_{0.9-x}$Eu$_x$Sr$_{0.1}$MnO$_3$ (*x*=0.000 (**A**), 0.025 (**B**)) sample as a function of temperature plots when the temperature is smaller than the Curie temperature (a) *Ms versus T* plot (b) *Ms(T)·(dMs/dT)$^{-1}$ versus T* plot, and the reciprocal zero-field magnetic susceptibility as a function of temperature plots (c) χ_0^{-1} *versus T* plot and (d) χ_0^{-1} *(dχ_0^{-1}/dT) versus T* plot

and γ > 1, indicating that the doping resulted in double exchange, which led to the increase in the magnetic field and the magnetic entropy change.

The isothermal magnetic entropy ΔS_M was generally calculated using Maxwell's thermodynamic equation. Then the magnetocaloric effects of the magnetic material were estimated as described previously [37–39]. The equations involved were as follows

$$\Delta S_M(T,H) = S_M(T,H) - S_M(T,0) = \int_0^H (\partial S/\partial H)dH \quad (11)$$

Substituting $(\partial S/\partial H)_T = (\partial M/\partial T)_S$ into Eq. (11), the following equation was obtained:

$$\Delta S_M(T,H) = S_M(T,H) - S_M(T,0) = \int_0^H \left[\partial M(T,H)/\partial T\right]dH \quad (12)$$

The magnetic entropy change of the polycrystalline sample La$_{0.9-x}$Eu$_x$Sr$_{0.1}$MnO$_3$ (*x*=0.000, 0.025) under different applied magnetic fields was obtained using Eq. (12). It is necessary to approximate Eq. (12) numerically because of discrete experimental data. This change of magnetic entropy of the polycrystalline samples was expressed as a function of temperature, as shown in Fig. 10. The results show that the magnetic entropy change increased as the applied magnetic field increased. The increase in the magnetic entropy change was attributed to the increased magnetic order of the samples and the applied magnetic field, which led to an increase in magnetization near T_c [1]. For the sample with *x*=0.000, a maximum magnetic entropy change was observed around 130 K. When the applied magnetic field reached 7 T, the maximum magnetic entropy was 2.76 ± 0.002 J· kg^{-1}· K^{-1}. For the second sample with *x*=0.025, the maximum magnetic entropy change was obtained near 125 K. The maximum magnetic entropy change was 2.81 ± 0.002 J· kg^{-1}· K^{-1} when the applied magnetic field reached 7 T. Small errors are introduced with the experimental magnetization data and the numerical approximation of Eq. (12). The increase in magnetic entropy after doping Eu^{3+} resulted from the decrease in the average ionic radius < r_A > of site A. Therefore, the lattice disorder increased, and the Mn–O-Mn bond angle was inhibited [3, 9, 40]. Furthermore, the spin–lattice coupling played an important role in the change of magnetic entropy

in the magnetic ordering, and the coupling strength changes as the average ionic radius of site A changed. Eu^{3+} doping reduced the < Mn–O–Mn > bond angle and increased the distortion of MnO$_6$ octahedron, which in turn weakened the interaction and affected the parallel arrangement of Mn^{3+}/Mn^{4+} spins. Therefore, there was a trend that the enhanced distortion tends to increase the spin–lattice coupling, which in turn increases the change in magnetic entropy [1, 8, 41].

Good magnetic refrigerating materials have a large ΔS_M and a high cooling efficiency (RC). RC is another critical parameter for magnetic refrigerating materials used in the field of magnetic refrigeration technology and was used to determine the performance of magnetic refrigerating materials [42, 43]. The definition of RC is as follows: RC=|− ΔS_M|·ΔT_{FWHM} where ΔT_{FWHM} is the full width at half maximum of the magnetic entropy of the magnetic entropy versus temperature plot. The RC of the La$_{0.9-x}$Eu$_x$Sr$_{0.1}$MnO$_3$ samples with *x*=0.000 and 0.025 at an applied magnetic field of 7 T are 436.01 ± 0.002 J· kg^{-1} and 438.09 ± 0.002 J· kg^{-1}, respectively. The comparison of the magnetocaloric parameters of La$_{0.9-x}$Eu$_x$Sr$_{0.1}$MnO$_3$ (*x*=0.000, 0.025) samples and similar magnetic refrigeration materials in a 5-T magnetic field is shown in Table 3. The magnetic entropy and RC of Gd are 9 J· kg^{-1}· K^{-1} and 405 J· kg^{-1} in a 5-T magnetic field, respectively. The results show that the La$_{0.9-x}$Eu$_x$Sr$_{0.1}$MnO$_3$ (*x*=0.000, 0.025) samples achieved magnetic refrigeration in the middle of the temperature curve and can, therefore, be used as good magnetic refrigerating molecules.

The ∆Tad is an important parameter for the magnetocaloric effect (MCE) of the magnetic materials. The relationship between the ∆Tad and the isothermal magnetic entropy change is represented by the following equation [44]:

$$\Delta T_{ad}(T)_{\Delta H} = -\int_{H_1}^{H_2} \frac{T}{C_{H,P}} \frac{\partial M(H,T)}{\partial T}dH = \frac{T}{C_{H,P}}\Delta S_M(T) \quad (13)$$

where $\Delta S_M(T)$ reveals the temperature-dependent magnetic entropy change; $C_{H,P}$ stands for the specific heat of the material in an applied magnetic field *H* at a constant pressure; the specific heat without an applied magnetic field is given by the following equation [45]:

$$C_{p,m} = 2.82 + 0.874T - \frac{6.93 \times 10^4}{T^2} + 398 \times 10^{-7} - 3.31$$
$$\times 10^{-2}T^{3/2} \quad (77 \leq T \leq 298) \quad (14)$$

The maximum adiabatic temperatures of both samples at an applied field of 7 T were obtained using Eqs. (13) and (14) and are $\Delta T_{ad}^{max}(T_{c1}) = 5.67 \pm 0.001K$ and $\Delta T_{ad}^{max}(T_{c2}) = 4.89 \pm 0.002K$, respectively. Figure 11 shows
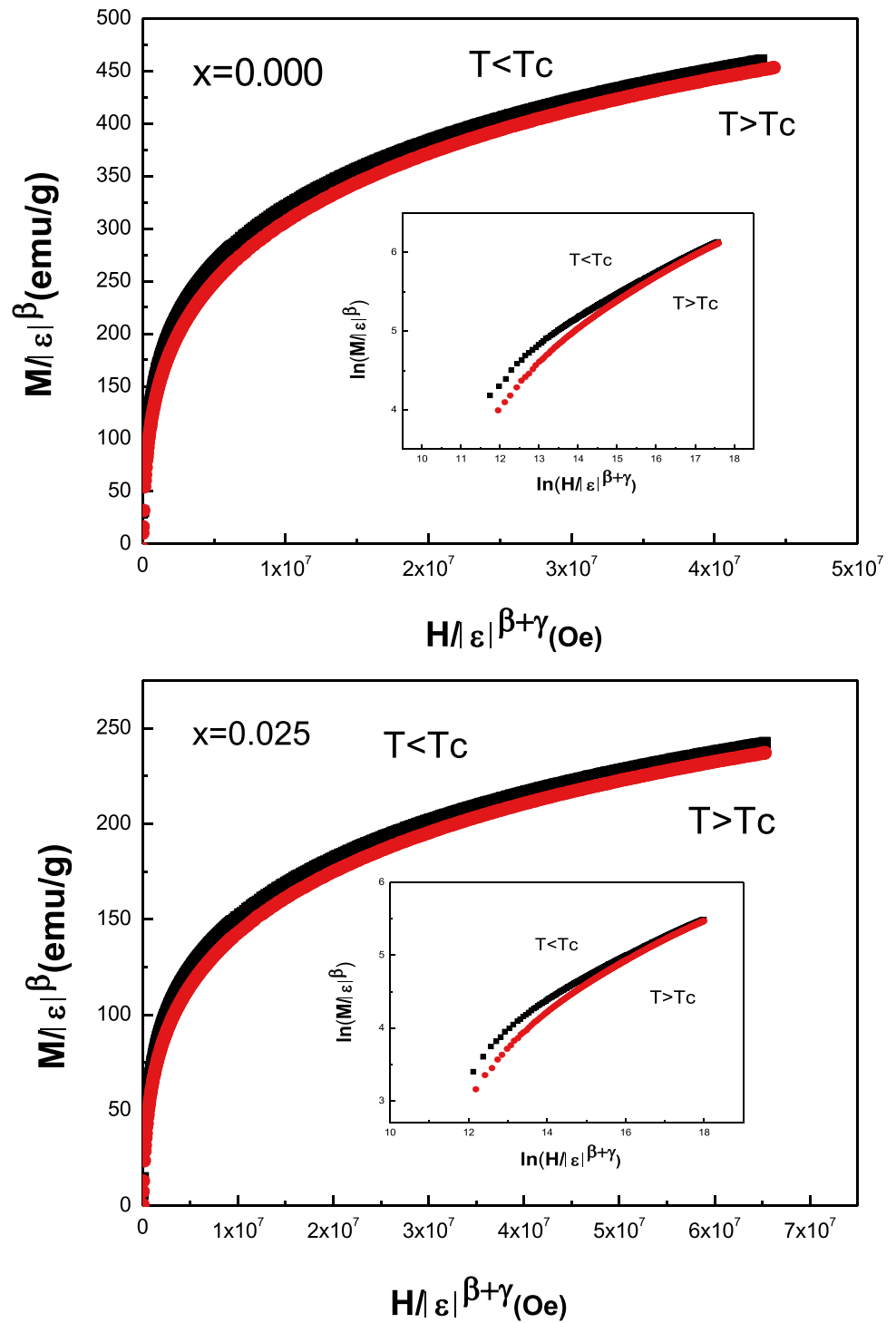
the maximum adiabatic temperature curves of both samples at the varied applied field. The trend of the change in the maximum adiabatic temperature (ΔT_{ad}^{max}) is similar to the trend of the maximum magnetic entropy change. Both the

maximum adiabatic temperature and the maximum magnetic entropy change increased as the applied field increased.

Based upon the rescaled magnetic entropy change curves, Franco et al. [46] hypothesized that the Fe-doped

Fig. 9 Temperature dependence of the exponent (*n*) of the change in magnetic entropy with different applied magnetic fields from 1 to 7 T
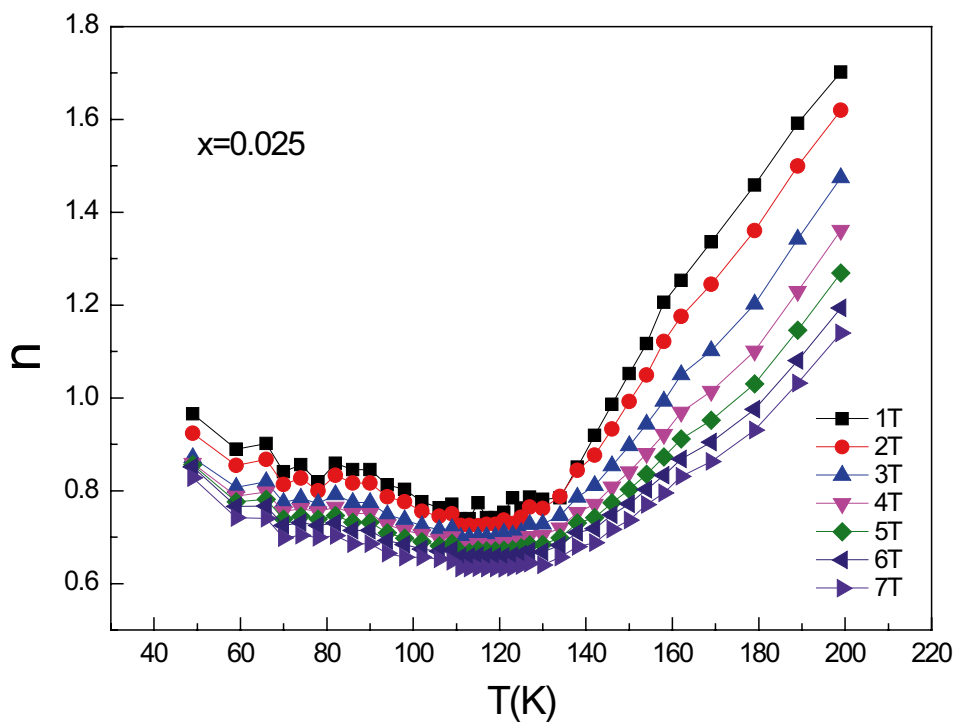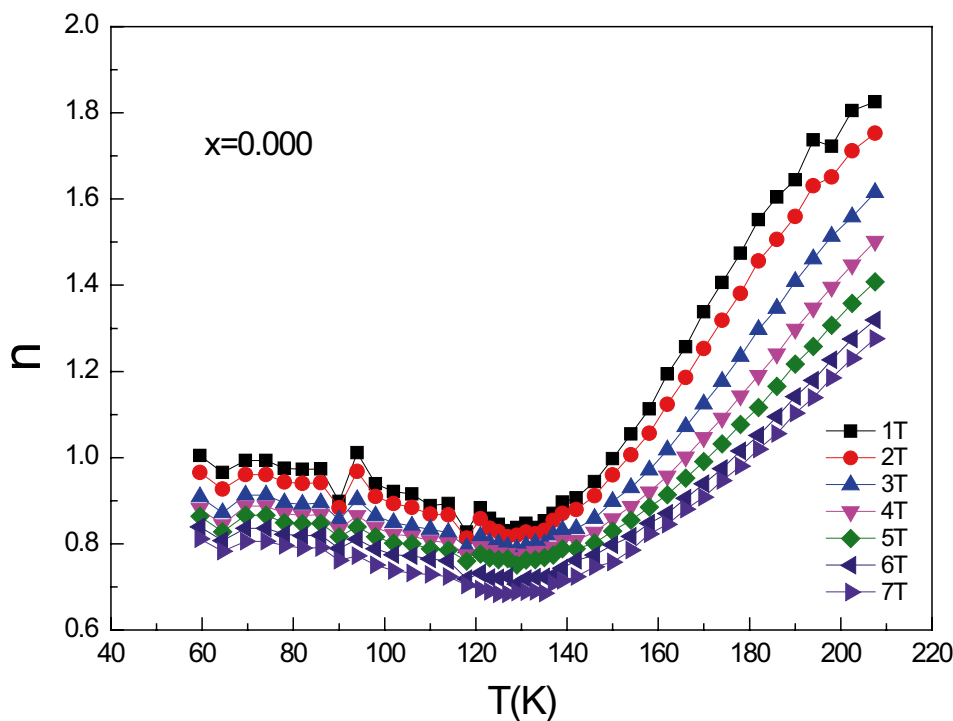

$Gd_5Ge_2Si_2$ underwent a second-order magnetic phase transition if the modified curve construction recollapsed the magnetic entropy change onto a single curve in a temperature range near the peak of the magnetic entropy change at different applied fields. The samples had a

first-order phase transition if the magnetic entropy change did not collapse to a single curve in a range of $T < T_C^{3D}$.

Figure 12 shows a rescaled magnetic entropy change plot of the $La_{0.9-x}Eu_xSr_{0.1}MnO_3$ ($x = 0.000, 0.025$) samples. The y-axis is the ratio of the magnetic entropy change

Fig. 10 The negative magnetic entropy change under the same applied magnetic field versus temperature ($-\Delta S\text{-}T$) plots for La$_{0.9-x}$Eu$_x$Sr$_{0.1}$MnO$_3$ samples with **a** $x=0.000$ and **b** $x=0.025$

(a) $x=0.000$

1T, 2T, 3T, 4T, 5T, 6T, 7T

(b)

1T, 2T, 3T, 4T, 5T, 6T, 7T
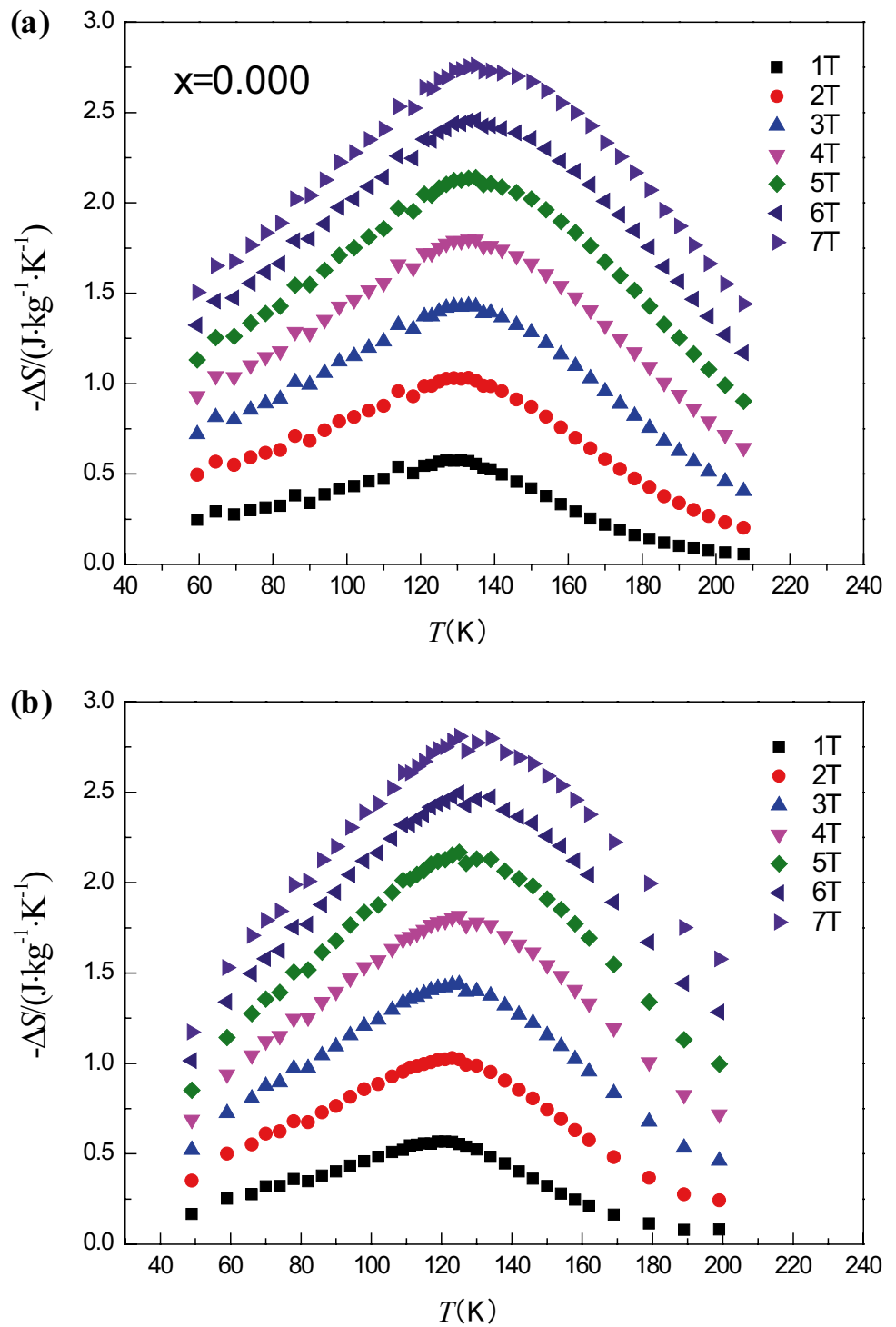
(ΔS) to the maximum magnetic entropy change (ΔS_M) at the applied fields. The x-axis is θ, which is defined as

$$\theta = \begin{cases} -\dfrac{T-T_c}{T_1-T_c} & T \leq T_c \\ \dfrac{T-T_c}{T_2-T_c} & T \geq T_c \end{cases} \tag{15}$$

where T_1 and T_2 stand for the two reference temperatures corresponding to $\Delta S_M/2$.

Figure 12 illustrates that the rescaled magnetic entropy change collapses to a single curve, indicating the occurrence of a second-order phase transition, which is in good agreement with the previous results.

Table 3 Comparison of the magnetocaloric parameters of La$_{0.9-x}$Eu$_x$Sr$_{0.1}$MnO$_3$ ($x=0.000$, 0.025) samples and similar magnetic refrigerant materials under a magnetic field of 5 T

Sample	T_C/K	$-\Delta S_M$/(J·kg^{-1}·K^{-1})	RC/(J·kg^{-1})	$\mu_0\Delta H$/T	Ref
La$_{0.9}$Sr$_{0.1}$MnO$_3$	130	2.76	295	5	Present work
La$_{0.875}$Eu$_{0.025}$Sr$_{0.1}$MnO$_3$	120	2.81	296	5	Present work
La$_{0.85}$Eu$_{0.05}$Sr$_{0.1}$MnO$_3$	121	1.95	268	5	[2]
(La$_{0.7}$Sm$_{0.3}$)$_{0.85}$K$_{0.15}$MnO$_3$	130	2.70	48	5	[16]
La$_{0.6}$Pr$_{0.1}$Ba$_{0.3}$MnO$_3$	94	1.48	-	5	[41]
La$_{0.7}$Te$_{0.3}$Mn$_{0.5}$Co$_{0.5}$O$_3$	220	2.2	121	5	[47]
La$_{0.7}$Sr$_{0.3}$Mn$_{0.8}$Fe$_{0.2}$O$_3$	94	1.3	168	5	[48]
La$_{0.67}$Sr$_{0.33}$MnO$_3$(48 nm)	275	1.09	133	5	[49]

Fig. 11 The field dependence of the maximum values of adiabatic temperature change ΔT_{ad}^{max}
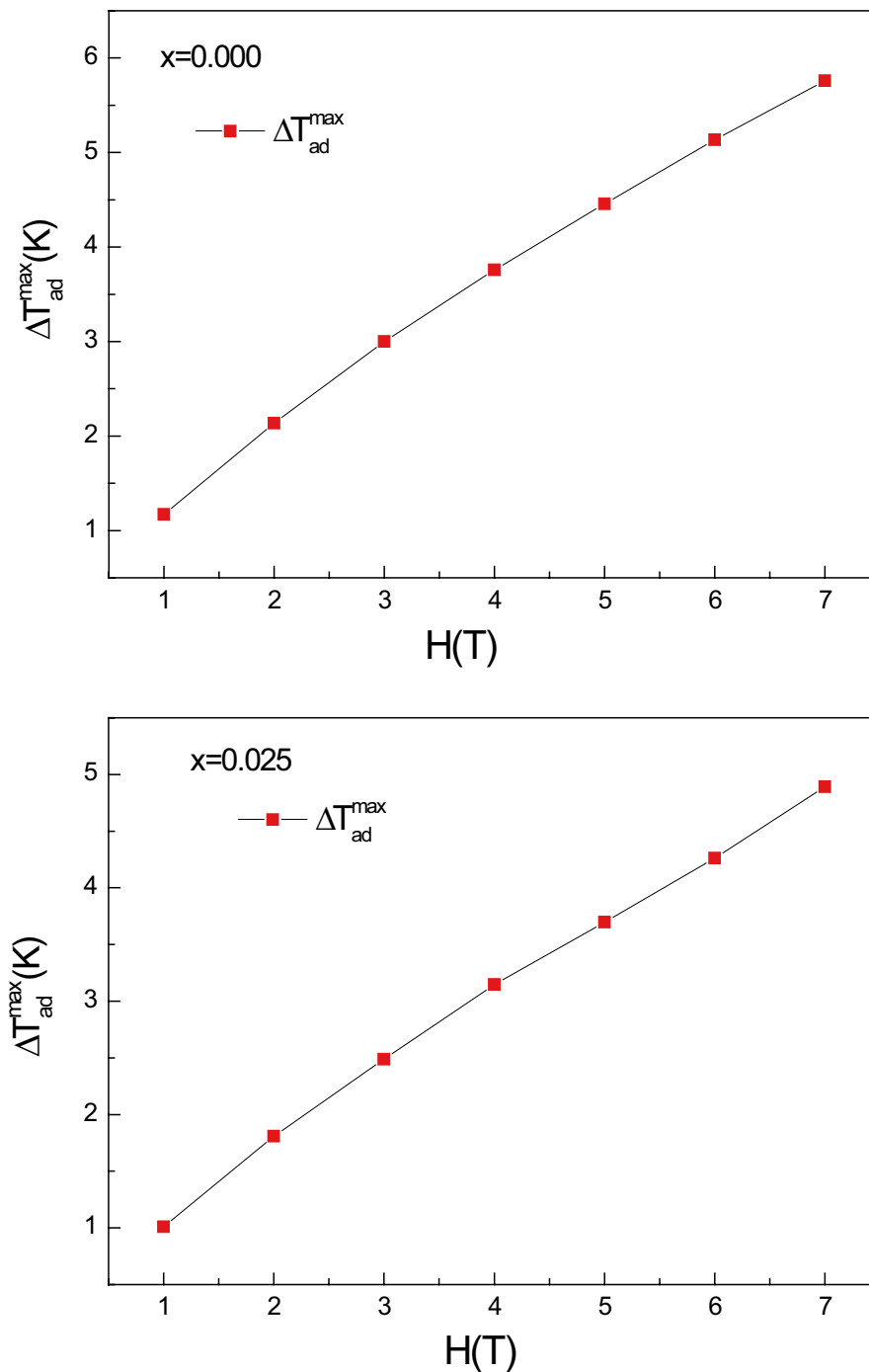
Fig. 12 Behavior of the master curve as a function of the rescaled temperature for different magnetic fields
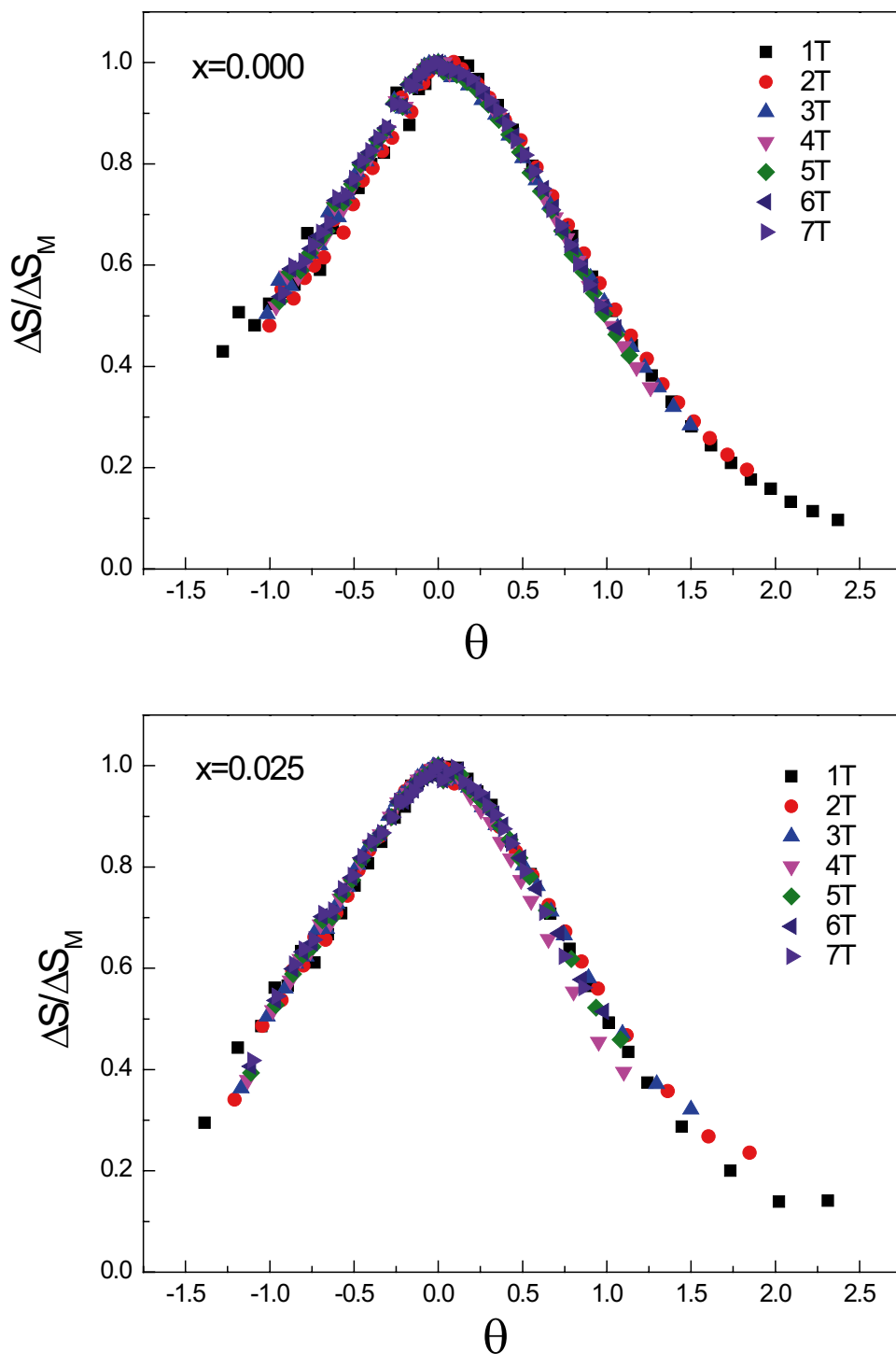
4 Conclusions

The effects of Eu^{3+} and Sr^{2+} cationic double-doping on the preformed clusters, critical behavior, and magnetic entropy change of two $LaMnO3$ samples were investigated. Our results show that the $La_{0.9-x}Eu_xSr_{0.1}MnO_3$ ($x = 0.000$, 0.025) polycrystalline samples we prepared

through a traditional solid-state reaction were unidirectional orthogonal crystal structure with the space group of *Pbnm*. As the temperature increased from 15 to 380 K, the two $La_{0.9-x}Eu_xSr_{0.1}MnO_3$ samples sequentially presented the characteristics of cluster spin glass, ferromagnetic phase, preformed cluster, and paramagnetic phase. The Curie temperatures of the two samples were 130 K

and 120 K, respectively. The phase transition of the two samples was the second-order phase transition, and the critical indexes of the samples were analyzed. The critical index of the sample with $x = 0.000$ was best fitted to the mean field model, and the critical index of the sample with $x = 0.025$ fit best with the 3D- Heisenberg model. At an applied magnetic field of 7 T and a temperature of 130 K, the maximum magnetic entropy changes of the two polycrystalline $La_{0.9-x}Eu_xSr_{0.1}MnO_3$ samples (with $x = 0.000$ and $x = 0.025$) were 2.76 ± 0.002 J$\cdot$ kg$^{-1}\cdot$ K^{-1} and 2.81 ± 0.002 J$\cdot$ kg$^{-1}\cdot$ K^{-1}, respectively, and the magnetic refrigerating capacities were 436.01 ± 0.002 J$\cdot$ kg^{-1} and 438.09 ± 0.002 J$\cdot$ kg^{-1}, respectively. Our results show that the magnetic entropy change and magnetic refrigerating capacities of the samples increased after doping. The results suggest that $La_{0.9-x}Eu_xSr_{0.1}MnO_3$ samples with $x = 0.000$ and 0.025 can be used as magnetic refrigerants in the medium temperature range of 80–250 K.

Declarations

Conflict of Interest The authors declare no competing interests.

References

1. Vadnala, S., Asthana S.: Magnetocaloric effect and critical field analysis in Eu substituted La0.7-xEuxSr0.3MnO3 (x=0.0, 0.1, 0.2, 0.3) manganites. J. Magn. Magn. Mater. **446**, 68 (2018)

2. Jin, X., Lu, Y., Sun, Y., Wu, H., Sun, X., Cao, F., Chen, H., Xu, B., Zhao, J.: Magnetic properties and magnetic entropy changes of Eu-doped La0.9Sr0.1MnO3 perovskite manganese oxides. J. Low Temp. Phys. **195**, (2019)

3. Anwar, M.S., Kumar, S., Ahmed, F., Arshi, N., Kim, G.W., Koo, B.H.: Above room temperature magnetic transition and magnetocaloric effect in La0.66Sr0.34MnO3. J. Korean Phys. Soc. **60**(10), 1587 (2012)

4. Bouderbala, A., Makni-Chakroun, J., Cheikhrouhou-Koubaa, W., Koubaa, M., Cheikhrouhou, A., Nowak, S., Ammar-Merah, S.: Structural, magnetic and magnetocaloric study of La0.7−xEuxSr0.3MnO3 (x=0.1, 0.2 and 0.3) manganites. Ceram. Int. **41**(6), 7337 (2015)

5. Debnath, J.C., Zeng, R., Kim, J.H., Chen, D.P., Dou, S.X.: Anisotropic and excellent magnetocaloric properties of La0.7Ca0.3MnO3 single crystal with anomalous magnetization. Mater. Sci. Eng. B. **177**(1), 48 (2012)

6. Yang, R.F., Sun, Y., Di, N.L., Li, Q.A., Cheng, Z.H.: Anisotropic and large low-field magnetic entropy change in a La4/3Sr5/3Mn2O7 single crystal. J. Magn. Magn. Mater. **309**(1), 149 (2007)

7. Koubaa W.C.R., Koubaa, M., Cheikhrouhou, A.: Structural, magnetotransport, and magnetocaloric properties of La0.7Sr0.3−xAgxMnO3 perovskite manganites. J. Alloys Compd. **453**(1), 42 (2008)

8. Liedienov, N.A., Pashchenko, A.V., Pashchenko, V.P., Prokopenko, V.K., Revenko, Y.F., Mazur, A.S., Sycheva, V.Y., Kamenev, V.I., Levchenko, G.G. Structure defects, phase transitions, magnetic resonance and magneto-transport properties of La0.6–xEuxSr0.3Mn1.1O3–δ ceramics. Low Temp. Phys. **42**(12), 1102 (2016)

9. Reshmi, C.P., Savitha Pillai, S., Vasundhara, M., Raji, G.R., Suresh, K.G., Raama Varma, M.: Co-existence of magnetocaloric effect and magnetoresistance in Co substituted La0.67Sr0.33MnO3 at room temperature. J. Appl. Phys. **114**(3), 033904 (2013)

10. Zhang, J., Yan, Q., Wang, F., Yuan, P., Zhang, P.: Field-induced transition in the layered manganite LaEu0.2Sr1.8Mn2O7. J. Phys. Condens. Matter. **13**(5), 917 (2001)

11. Hamad, M.A.: Magnetocaloric effect in La0.65−xEuxSr0.35MnO3. Phase Trans. **87**(5), 460 (2014)

12. Carretero-Genevrier, A., Frontera, C., Hassini, A., Oro-Sole, J., Moreno, C., Obradors, X., Puig, T., Mestres, N.: Chemical solution growth of La0.7Sr0.3MnO3 nanotubes in confined geometries. J. Sol-Gel Sci. Techn. **73**(3), 620 (2015)

13. Xing, R., Zhao, J.J., Lu, Y., Wu, H.Y., Zheng, L., Sun, Y., Cheng, Z.H.: Effect of Ca doping on the magnetic properties of Nd0.5Sr0.5MnO3 studied by electron spin resonance. Phys. B Condens. Matter. **406**(24), 4569 (2011)

14. Chen, X.J., Soltan, S., Zhang, H., Habermeier, H.U.: Strain effect on electronic transport and ferromagnetic transition temperature in La0.9Sr0.1MnO3 thin films. Phys. Rev. B Condens. Matter Mate. Phys. **65**, 1744021 (2002)

15. Vadnala, S., Pal, P., Asthana, S.: Influence of A-site cation disorder on structural and magnetocaloric properties of Nd0.7−xLaxSr0.3MnO3 (x=0.0, 0.1, 0.2 & 0.3). J. Rare Earth. **33**(10), 1072 (2015)

16. Akça, G., Çetin, S., Ekicibil, A.: Structural, magnetic and magnetocaloric properties of (La 1-x Sm x) 0.85 K 0.15 MnO 3 (x = 0.0, 0.1, 0.2 and 0.3) perovskite manganites. Ceram. Int. **43**, (2017)

17. Daivajna, M.D., Kumar, N., Awana, V.P.S., Gahtori, B., Christopher J.B., Manjunath, S.O., Syu, K.Z., Kuo, Y.K., Rao, A.: Electrical, magnetic and thermal properties of Pr0.6−xBixSr0.4MnO3 manganites. J. Alloys Compd. **588**, 406 (2014)

18. Tang, Y.K., Sun, Y., Cheng, Z.H.: Cooling field dependence of exchange bias in phase-separated La0.88Sr0.12CoO3. J. Appl. Phys. **100**(2), 023914 (2006)

19. Saravanan, C., Thiyagarajan, R., Manikandan, K., Sathiskumar, M., Kanjariya, P.V., Bhalodia, J.A., Arumugam, S.: Effect of Cd doping on magnetocaloric effect and critical behavior analysis on perovskite Nd1−xCdxMnO3 (x = 0, 0.1, 0.2, 0.3, and 0.4) manganite polycrystals. J. Appl. Phys. **122**(24), 245109 (2017)

20. Freitas, R.S., Mitchell, J.F., Schiffer, P.: Magnetodielectric consequences of phase separation in the colossal magnetoresistance manganite Pr0.7Ca0.3MnO3. Phys. Rev. B. **72**(14), 144429 (2005)

21. Das, D., Chowdhury, P., Das, R.N., Srivastava, C.M., Nigam, A.K., Bahadur, D.: Solution sol–gel processing and investigation of percolation threshold in La2/3Ca1/3MnO3:xSiO2 nanocomposite. J. Magn. Magn. Mater. **238**(2), 178 (2002)

22. Thanh, T.D., Linh, D.C., Manh, T.V., Ho, T.A., Phan, T.L., Yu, S.C.: Coexistence of short- and long-range ferromagnetic order in La0.7Sr0.3Mn1−xCoxO3 compounds. J. Appl. Phys. **117**(17), 17C101 (2015)

23. Nisha, P., Pillai S.S., Suresh, K.G., Varma, M.R.: Influence of Dy addition on the magnetocaloric effect of

La0.67Ca0.33Mn0.9V0.1O3 ceramics. J. Magn. Magn. Mater. **324**(1), 37 (2012)

24. Tang, Y.K., Ma, X., Kou, Z.Q., Sun, Y., Di, N.L., Cheng, Z.H., Li, Q.A.: Slight La doping induced ferromagnetic clusters in layered La3–3x Sr1+3x Mn3 O10 (x=1.00,0.99,0.95). Phys. Rev. B. **72**, (2005)

25. Punith Kumar, V., Dayal, V.: Critical behavior and non-universal low-field magnetic scaling in La1-xBixMnO3 (x=0.4 & 0.6) perovskite manganite oxide. AIP Conf. Proc. **1665**(1), 030014 (2015)

26. Phan, M.H., Srinivas, V., Yu, S.C., Hur, N.H.: Magnetic frustration effects in LaCaMnO3 single crystals. J. Appl. Phys. **93**(10), 8200 (2003)

27. He, C., Torija, M.A., Wu, J., Lynn, J.W., Zheng, H., Mitchell, J.F., Leighton, C.: Non-Griffiths-like clustered phase above the Curie temperature of the doped perovskite cobaltite La1-xSrxCoO3. Phys. Rev. B. **76**(1), 014401 (2007)

28. Tlili, R., Omri, A., Bekri, M., Bejar, M., Dhahri, E.: Effect of Ga substitution on magnetocaloric effect in La0.7(Ba, Sr)0.3Mn1−xGaxO3 (0.0≤ x ≤0.20) polycrystalline at room temperature. J. Magn. Magn. Mater. **399**, (2015)

29. Jeen, H., Javed, R., Biswas, A.: Growth of atomically flat thin films of the electronically phase-separated manganite (La0.5Pr0.5)0.67Ca0.33MnO3. Appl. Phys. A. **122**, (2016)

30. Wang, B., Zhao, X., Wu, A., Cao, S., Xu, J., Kalashnikova, A.M., Pisarev, R.V.: Single crystal growth and magnetic properties of Sm0.7Tb0.3FeO3 orthoferrite single crystal. J. Magn. Magn. Mater. **379**, 192 (2015)

31. Liao, D.Q., Sun, Y., Yang, R.F., Cheng, Z.H.: Structural, magnetic, and electrical properties of La1−NdxMn0.8Cr0.2O3 (x⩽0.3). Phys. B Condens. Matter. **394**(1), 104 (2007)

32. Mira, J., Rivas, J., Rivadulla, F., Vázquez-Vázquez, C., López-Quintela, M.A.: Change from first to second order magnetic phase transition in La2/3(Ca, Sr)1/3MnO3 perovskites. Phys. Rev. B. **60**(5), 2998 (1999)

33. Yang, R.F., Sun, Y., Ma, X., Tang, Y.K., Li, Q.A., Cheng, Z.H.: Colossal electroresistance and low-field colossal magnetoresistance in the single-crystal bilayered manganite La1.2 Sr1.8 Mn2 O7. Phys. Rev. B. **73**, (2006)

34. Tka, E., Cherif, K., Jemai, D., Dhahri, E., Belmabrouk, H.: Effect of Al substitution on magnetocaloric effect in La0.57Nd0.1Sr0.33Mn1−xAlxO3 (0.0 ≤ x ≤ 0.30) polycrystalline near room temperature. J. Alloys Compd. **518**, 32 (2012)

35. Lampen, P.J., Zhang, Y., Phan, T.L., Zhang, P., Yu, S.C., Srikanth, H., Phan, M.H.: Magnetic phase transitions and magnetocaloric effect in La0.7Ca0.3Mn1-xFexO3 0.00≤ x ≤0.07 manganites. J. Appl. Phys. **112**(11), 113901 (2012)

36. Yu, B., Sun, W., Fan, J., Lan, X., Zhang, W., Zhu, Y., Han, H., Zhang, L., Ling, L., Yang, H.: Scaling study of magnetic phase transition and critical behavior in Nd0.55Sr0.45Mn0.98Ga0.02O3 manganite. Mater. Res. Bull. **99**, 393 (2018)

37. Arayedh, B., Kallel, S., Kallel, N., Peña, O.: Influence of non-magnetic and magnetic ions on the MagnetoCaloric properties of La0.7Sr0.3Mn0.9M0.1O3 doped in the Mn sites by M=Cr, Sn, Ti. J. Magn. Magn. Mater. **361**, 68 (2014)

38. Phan, M.H., Peng, H.X., Yu, S.C., Hur, N.: Large magnetic entropy change above 300K in a La0.7Ca0.2Sr0.1MnO3 single crystal. J. Magn. Magn. Mater. **290–291**, 665 (2005)

39. Guo, Z.B., Zhang, J.R., Huang, H., Ding, W.P., Du, Y.W.: Large magnetic entropy change in La0.75Ca0.25MnO3. Appl. Phys. Lett. **70**(7), 904 (1997)

40. Kumar, V.S., Chukka, R., Chen, Z., Yang, P., Chen, L.: Strain dependent magnetocaloric effect in La0.67Sr0.33MnO3 thin-films. AIP Adv. **3**(5), 052127 (2013)

41. Cherif, R., Ellouze, M., Elhalouani, F., Obbade, S.: Study of magnetic and magnetocaloric properties of La0.6Pr0.1Ba0.3MnO3 and La0.6Pr0.1Ba0.3Mn0.9Fe0.1O3 perovskite-type manganese oxides. J. Mater. Sci. **49**, (2014)

42. Ulyanov, A.N., Kim, J.S., Kang, Y.M., Yoo, D.G., Yoo, S.I.: Oxygen deficiency as a driving force for metamagnetism and large low field magnetocaloric effect in La0.7Ca0.3−xSrxMnO3−δ manganites. J. Appl. Phys. **104**(11), 113916 (2008)

43. Krichene, A., Boujelben, W., Cheikhrouhou, A.: Structural, magnetic and magnetocaloric properties in La0.5−xRexCa0.5MnO3 manganites (x=0; 0.1 and Re=Gd, Eu and Dy). J. Alloys Compd. **550**, 75 (2013)

44. Su, Y.: Magnetocaloric effect and critical behavior od perovskite-type rare-earth Titanate crystals. Doctoral dissertation, Harbin Institute of Technology.

45. Satoh, H., Takagi, M., Kinukawa, K.I., et al.: Heat capacity of LaMnO3. Thermochim. Acta **299**(1–2), 123–126 (1997)

46. Franco, V., Conde, A., Provenzano, V., Shull, R.D.: Scaling analysis of the magnetocaloric effect in Gd5Si2Ge1.9X0.1 (X=Al, Cu, Ga, Mn, Fe, Co). J. Magn. Magn. Mater. **322**(2), 218 (2010)

47. Uthaman, B., Anand, K., Rajan, R., Kyaw, H., Thomas, S., Al-Harthi, S., Suresh, K., Varma, M.R.: Structural properties, magnetic interactions, magnetocaloric effect and critical behaviour of cobalt doped La0.7Te0.3MnO3. RSC Adv. **5**, 86144 (2015)

48. Barik, S.K., Krishnamoorthi, C., Mahendiran, R.: Effect of Fe substitution on magnetocaloric effect in La0.7Sr0.3Mn1−xFexO3 (0.05≤x≤0.20). J. Magn. Magn. Mater. **323**(7), 1015 (2011)

49. Baaziz, H., Tozri, A., Dhahri, E., Hlil, E.K.: Magnetocaloric properties of La0.67Sr0.33MnO3 tunable by particle size and dimensionality. Chem. Phys. Lett. **691**, 355 (2018)